33RD CONGRESS
OF THE INTERNATIONAL COUNCIL
OF THE AERONAUTICAL SCIENCES
STOCKHOLM, SWEDEN, 4-9 SEPTEMBER, 2022

ICAS 2022 SWEDEN

RVE-BASED HOMOGENIZATION OF ADDITIVELY MANUFACTURED POROUS METALS

Alaimo, A.[1], Mantegna, G.[*1], Orlando, C.[1], Tumino, D[1] & Vindigni, C. R.[1]

[1]Faculty of Engineering and Architecture, Kore University of Enna, Cittadella Universitaria, 94100 Enna, Italy

Abstract

Additive Manufacturing technologies have been extensively used in different industry sectors thanks to the optimisation of material waste, reduction of the high production costs and the ability to create components with complex geometric shapes and highly customisable mechanical performance. However, to fully exploit the benefits of these technologies, in-depth knowledge is needed on how internal defects condition the overall behaviour of the component. In this work, a Representative Volume Element like approach is presented to study, through different numerical analyses, the effect of size, number and spatial distribution of micro-voids on the stress-strain behaviour of Selective Laser Melting additive manufactured AlSi10Mg. An in-house code on the commercial software ANSYS Parametric Design Language APDL is used to model a random pore distribution inside the RVE in compliance with statistical distribution retrieved from the literature; comparison with reference case studies are reported.

Keywords: Porosity, FEM, AdditiveManufacturing, RVE

1. Introduction

Additive Manufacturing (AM) technologies are spreading in multiple industry sectors thanks to their ability to reduce material waste and create complex geometries in one single process with high customisable mechanical properties. Starting from a digital CAD model, AM technologies create complex 3D components by stacking material layer-by-layer.

Among all AM technologies, powder bed melting processes such as Selective Laser Melting (SLM) allow maximum flexibility and geometric accuracy. More specifically, SLM is often considered the most attractive AM technique due to the possibility of using an extensive range of materials and tailoring specific properties based on the usage requirements at a relatively low cost. According to Aboulkhair et al. [1], SLM technologies allow to create monolithic parts with a weight reduction of up to 50 % with virtually no material waste.

Different factors such as powder quality and process parameters can drastically modify the overall behaviour and, despite being built layer by layer from fine powders and in an inert atmosphere, can intrinsically induce defects inside the component. Furthermore, it has been shown that different materials processed with different additive manufacturing technologies are more vulnerable to specific defects than others. For instance, aluminium processed with wire arc additive manufacturing technology is more prone to porosity defects than titanium which suffers more oxidation problems [2]. The scientific and industry communities are deeply involved developing multiple techniques to optimise the behaviour of AM products, such as in-situ monitoring and AI-optimised process parameters [3–7]. This increased knowledge can gradually shift the use of AM technologies from secondary to primary structures.

It is well known that internal defects such as micro-voids, cavities, and unfused powders constitute sites of initiation of cracks which significantly modify the fatigue life of the components; Odegard and Pedersen [8] showed that porosity of 1% in volume fraction in the AlSi7Mg alloy can lead to a reduction of 50% in the component fatigue life. Several efforts are constantly placed on modelling

their general behaviour to produce accurate and significant results. However, such a level of detail would be computationally unsustainable and, for this reason, a homogenisation approach is generally used. The Representative Volume Element (RVE) is first used to consider the micro-scale heterogeneity effects and, after a homogenisation process, the overall macro-scale mechanical response is retrieved in the so-called "micro-to-macro" modelling approach [9, 10]. Figure 1 shows the homogenisation process through the Representative Volume Element.

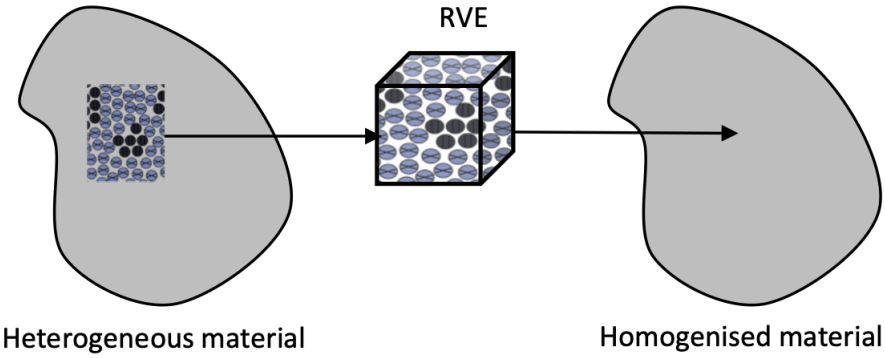

Figure 1 – Homogenisation process through the Representative Volume Element

Several definitions and properties of the RVE are given in the literature. According to Drugan and Willis [11], the RVE is defined as the smallest volume element capable of statistically representing the overall constitutive response of the material with errors lower than 5%. Furthermore, it must be structurally representative of the entire material with sufficient heterogeneity so that the overall apparent moduli are "macroscopically uniform" and independent of surface tension and displacement values [12]. The micro-meso-macro principle suggests a size smaller than the macroscopic body but sufficiently large to include its microstructure effects [13]. According to Gitman et al. [14], the RVE must be smaller than the overall macro-scale domain and yet sufficiently large compared to the micro-defects considered for the analysis.

The Representative Volume Element approach has been extensively used in the literature. Drugan and Willis [11] proposed a variational nonlocal macroscopic constitutive model used to estimate the minimum RVE size. Gusev [15] generated composite disordered unit cells through Monte Carlo runs. A finite element code based on a constant-strain-tetrahedra displacement method was used to retrieve the overall elastic constants. Only non-overlapping identical spheres were considered. Chan et al. [10] predicted the stress-strain behaviour of SS316L cast specimens with micro-voids through an RVE multiscale approach. In their work, the RVE considered a single pore with different shapes and positions. The effect of randomly distributed micro-inclusions with different sizes and shapes on the fretting fatigue behaviour in aluminium alloy 2024-T3 was studied through FEM-RVE analysis by Deng et al. [16]. Takezawa et al. [17] used the RVE for calculating the effective thermal conductivity of a porous metal with an optimized pore structure. Biswas and Ding [18] used a 2D RVE to characterise the deformation and fracture behaviour of porous titanium alloy processed by Laser Engineered Net Shaping. In their study the authors considered different shapes and distributions varying from a single centred pore to a regular matrix distribution. The study showed pores could serve both as a failure initiator and inhibitor. Later, Kanit et al. [19] used FEM-RVE analysis to determine the minimum RVE size introducing the integral range to relate the error estimation with the RVE size. Liu and Chen [20] used the finite element method with a 3D nanoscale RVE to determine the effective mechanical properties of Carbon nanotubes composites.

In this work, a Representative Volume Element like approach is used to study, through different numerical analyses, the effect of size, number and spatial distribution of micro-voids on the stress-strain behaviour of Selective Laser Melting additive manufactured AlSi10Mg. An in-house code on the commercial software ANSYS Parametric Design Language APDL is used to model different micro-voids configurations. Ultimately, a random pore distribution inside the RVE in compliance with statistical distribution retrieved from the literature is considered; comparisons with reference case studies are reported.

2. Representative Volume Element and Finite Element approach

Accurate analyses cannot underestimate material microstructure and internal micro-defects. However, numerical analyses of the whole domain are computationally unsustainable. For this reason, micro-to-macro modelling approaches through a Representative Volume Element have been extensively used to avoid such complex analyses. The homogenised properties obtained from the RVE analyses are used for the macro-scale analysis.

In this work, all the Representative Volumes Elements are assumed of cubic shape whereas pores are modelled as spheres. Different RVE configurations have been investigated. A single pore (SP) centred within the RVE was considered at first. Subsequently, RVEs with pores positioned in a regular matrix (MD) and with a completely random distribution (RD) were analysed. Random porosity distribution simulations allow overlap and intersection of spheres of different radii, thus simulating the coalescence of micro-voids during the manufacturing process. Figures 2a, 2b and 2c show RVE samples with different porosity distributions: No porosity (bulk), regular Matrix pore Distribution, and Random pore Distribution.

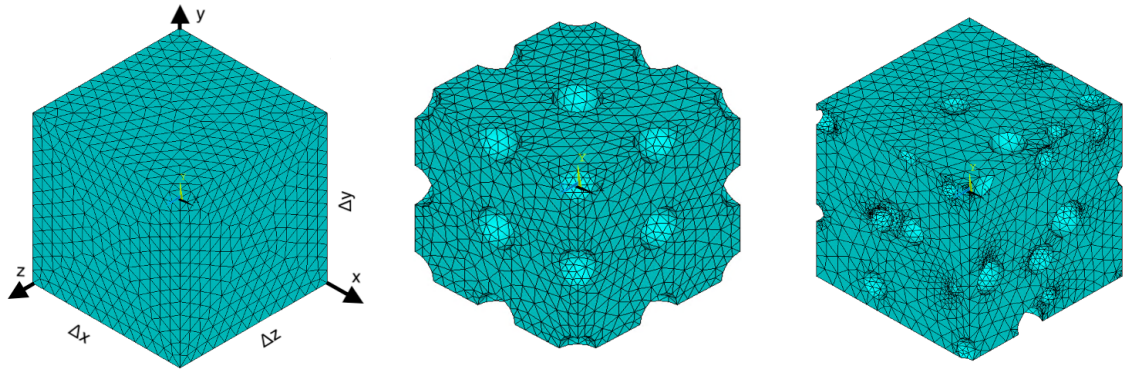

(a) (b) (c)

Figure 2 – Representative Volume Element. 2a Bulk, 2b MD: regular Matrix pore Distribution, 2c RD: Random pore Distribution.

The pre-processing phase is conducted in the Ansys Parametric Design Language (APDL) mechanical environment to create multiple RVE geometries in batch mode while controlling multiple parameters, such as its configuration and dimensions and the overall porosity. A custom routine was developed to generate the RVEs geometries.

Table 1 – RVE Boundary Conditions

	u_x	u_y	u_z
Face $yz_{\|x=0}$	0	free	free
Face $xz_{\|y=0}$	free	0	free
Face $xy_{\|z=0}$	free	free	0
Face $xz_{\|y=dy}$ coupled Rp1 y direction			
Face $xy_{\|z=dz}$ coupled Rp2 z direction			

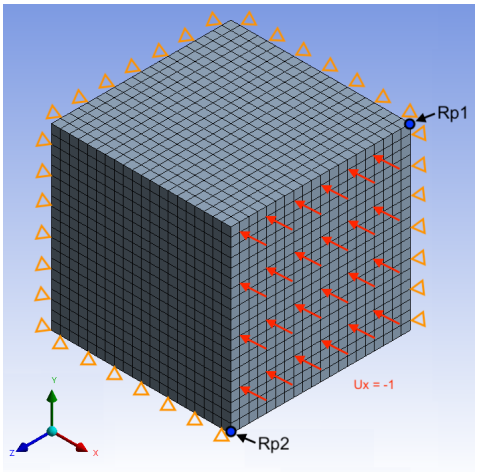

Figure 3 – RVE Boundary Conditions

The flowchart diagram to generate an RVE with a random distribution porosity is schematically shown in Figure 4. Spheres with different radii are progressively removed from the bulk volume until the desired porosity is reached. These spheres, randomly placed in the RVE, can overlap creating irregular shapes simulating pores coalescence.
The finite element analysis considers a compressive displacement loading applied on the right outer face ($x = \Delta x$) as shown in Figure 3. By taking advantage of the symmetry of the load, three symmetry planes are imposed. Furthermore, two faces are constrained to remain flat during the load through two remote points. Table 1 summarises the imposed boundary conditions.

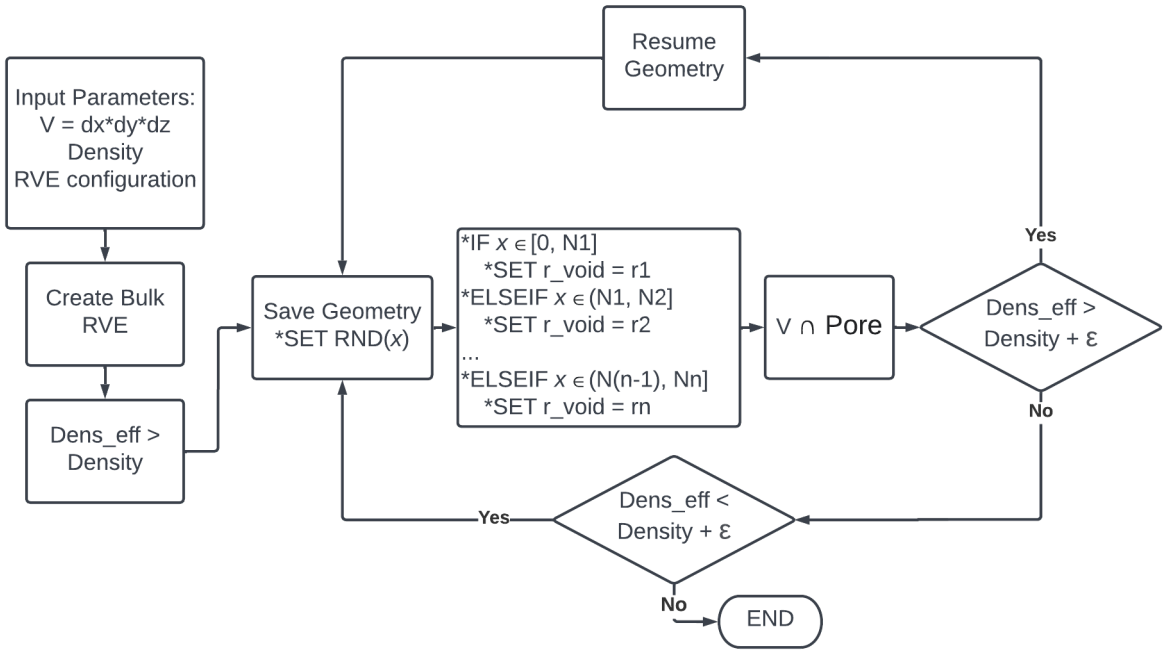

Figure 4 – Schematic flowchart diagram to generate RVEs geometries.

Quadratic, 10-node elements *"TET10"* are used to mesh the models. Curvature and proximity features have been included to improve the overall quality of the mesh.
In this early stage, a bilinear hardening law was used for the material constitutive model to describe the stress-strain relationship of a Selective Laser Melted AlSi10Mg.
The mechanical properties assumed for the numerical simulations are: Elastic modulus $E = 58GPa$, Poisson's ratio $\nu = 0.3$, Yield stress $\sigma_{yield} = 279MPa$ and Tangent modulus $E_T = 2830MPa$. Pores size and distributions are modelled according to literature references [21].
AlSi10Mg components produced with modern additive manufacturing technology behave nearly to bulk materials with a maximum porosity, depending on the process parameters, of 5% [1, 21–23]. For this reason, the numerical campaigns are limited from 0% (perfectly bulk material) to 5% volume fraction porosity. According to Yin et al. [24], volume fraction porosity is one of the main parameters that influence the mechanical behaviour in the linear region and for the initial yield stress. For this reason, a maximum error of 0.5% between the effective overall porosity and the desired porosity is imposed.

3. Results and discussion

Single pore centred in the RVE is considered first. Figure 5 compares true stress-strain curves of the SLM AlSi10Mg with different porosity from 0% (perfectly bulk material) to 5% volume fraction porosity. An RVE cube with a $2mm$ edge was used. As expected, porosity reduces both the elastic modulus and the yield strength.

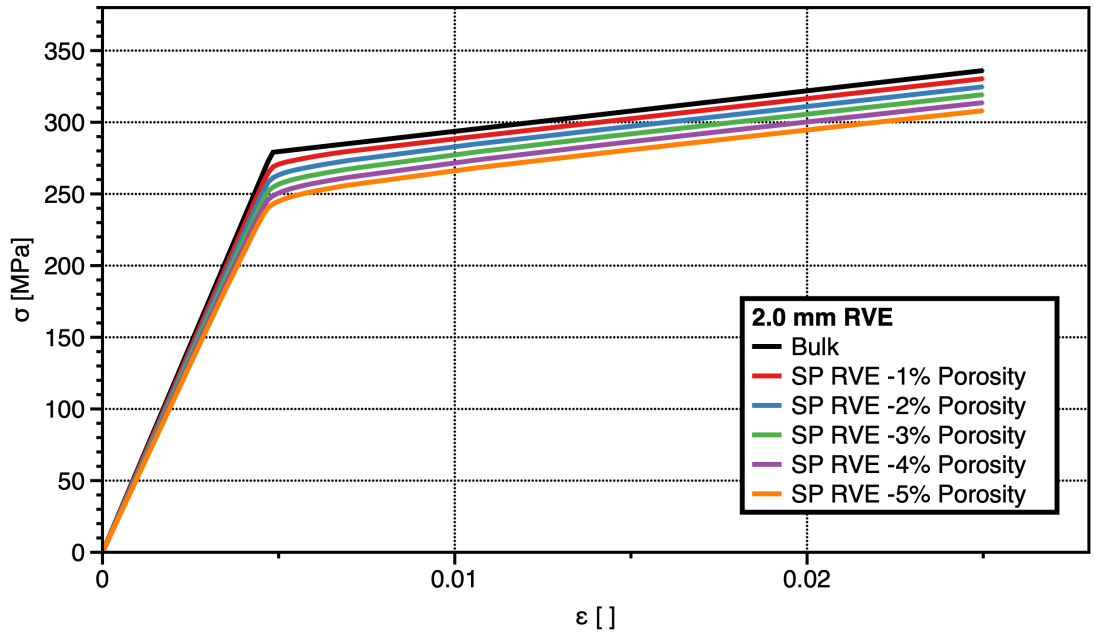

Figure 5 – Single Pore: True stress-strain curves. Bulk to 5% porosity.

The linear and quadratic fit of the effective and bulk elastic moduli ratio E/E_b as a function of the overall porosity v_p is shown in Figure 6. Linear fit can be approximated as Equation 1 with errors under 0.3%.

$$E = (1 - 2 * v_p) * E_b \tag{1}$$

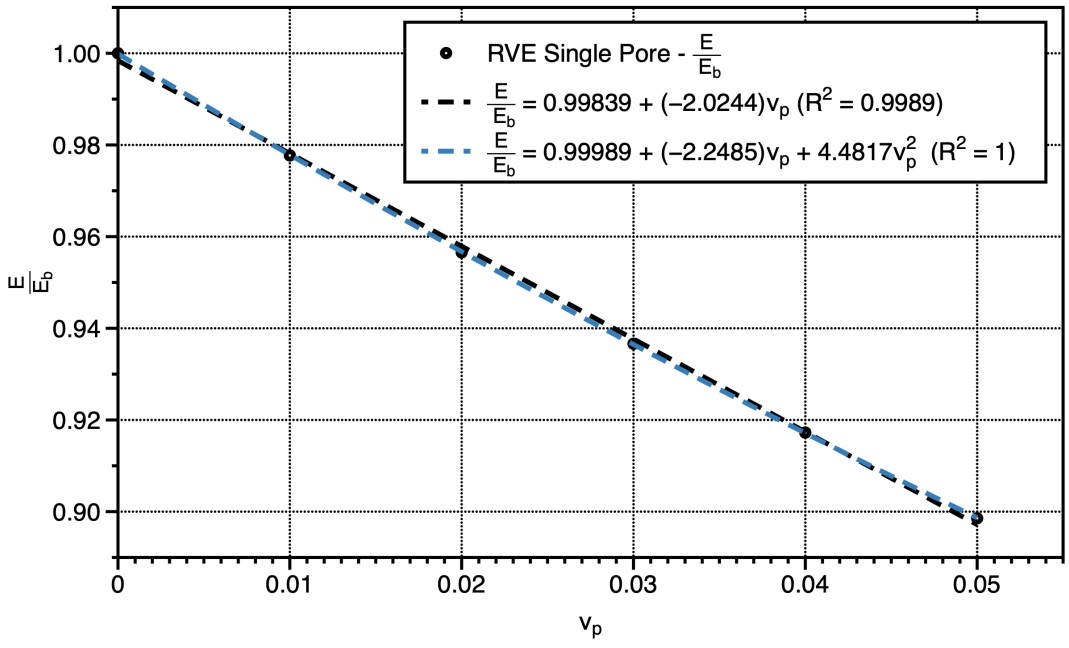

Figure 6 – RVE Single Pore: E/E_{bulk} vs v_p linear and quadratic fit.

Young's module and yield strength values with increasing porosity v_p are reported in Table 2. The yield stress σ_{yield} is retrieved from the stress-strain curves as the tension measured when the error between the numerical strain and the strain obtained by the purely elastic law exceeds a value of 2%, as shown in Figure 7.

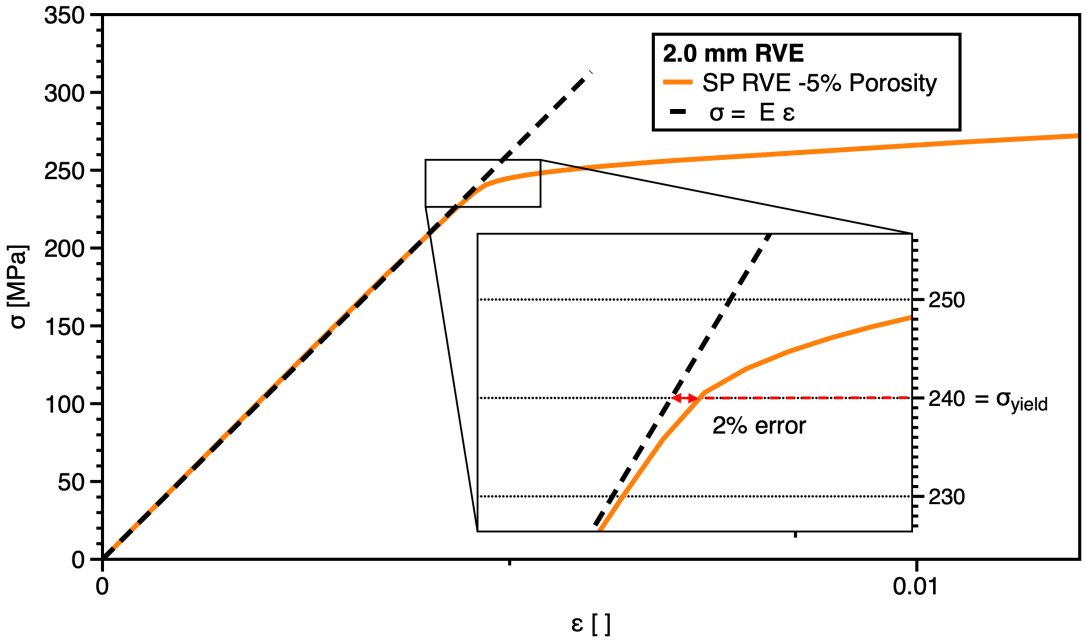

Figure 7 – Yield strain estimation detail.

Table 2 – RVE Single Pore: Elastic modulus and yield strength.

ν_p %	E_{SP} [MPa]	$\sigma_{yield\,SP}$ [MPa]
0%	58000	279
1%	56700	268
2%	55500	259
3%	54300	253
4%	53200	246
5%	52100	240

Next, the interaction of multiple pores of the same dimensions placed in a regular tridimensional matrix was studied. Pores diameters are functions of the chosen matrix (2x2x2, 3x3x3, 4x4x4) and the overall desired porosity. Figure 2b shows an RVE with pores in a 3x3x3 regular matrix.
The regular matrix distribution confirmed the mechanical properties degradation with increasing porosity recorded in the single pore distribution. Furthermore, it is interesting to notice that as the overall porosity increases, the mechanical response between the single pore and the regular matrix distribution slightly diverges, as shown in Figure 8. More specifically, a single centred pore inside the RVE makes it less stiff and has yield strength moderately lower than a configuration with multiple pores. Table 3 reports the elastic module and yield strength values of a regular matrix pore distribution 3x3x3. The error percentage of these values compared to the single pore distribution is also reported.

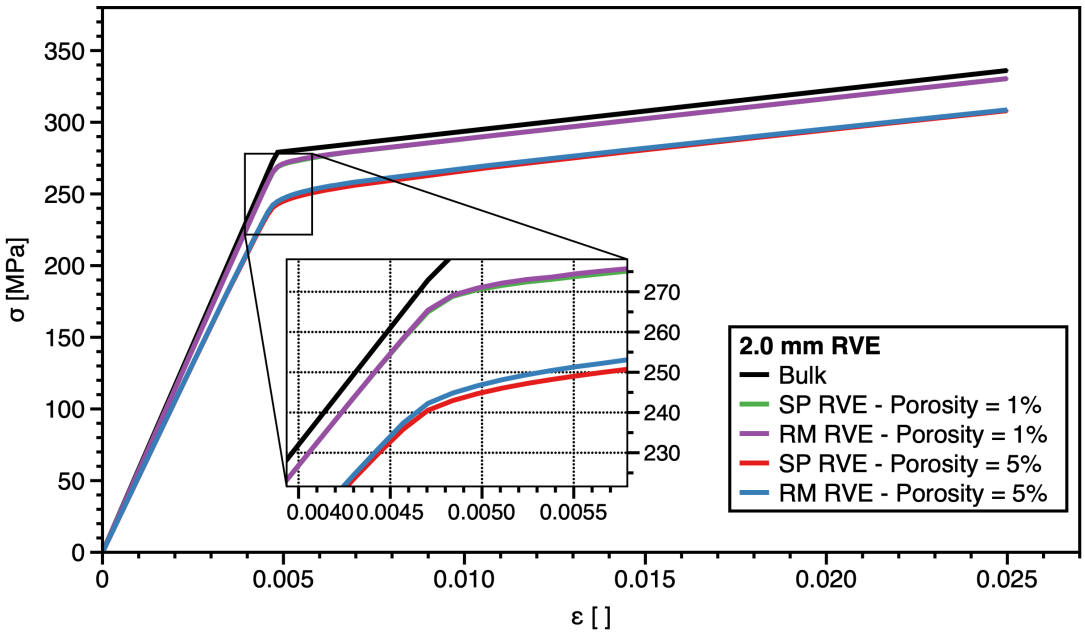

Figure 8 – RVE Single pore and RVE Regular matrix 3x3x3 stress-strain behaviour comparison.

Table 3 – RVE regular Matrix Distribution: Elastic modulus and yield strength.

v_p %	E_{MD} [MPa]	σ_{MD} [MPa]	$100\frac{E_{MD}-E_{SP}}{E_{SP}}$	$100\frac{\sigma_{MD}-\sigma_{SP}}{\sigma_{SP}}$
1%	56900	269	0.35%	0.37%
2%	55800	260	0.54%	0.39%
3%	54700	254	0.74%	0.40%
4%	53700	247	0.94%	0.41%
5%	52700	242	1.15%	0.83%

As already mentioned, the previous analyses confirm that overall volume fraction porosity is one of the main factor of influence for the linear mechanical behaviour of the models.
Finally, to study the interaction of coalesced pores, an RVE with a random pores distribution was investigated. As previously mentioned, different radii spheres are randomly placed inside the RVE, and their overlap simulates the coalescence of pores. An overall porosity of 3.16 % is selected for the random pores distribution analysis. The reference distribution is taken from Cai et al. [21] where pore size-frequency is given as a function of the pore size. Figure 9 compares the reference distribution with the numerical statistical distribution obtained at increasing RVE edge sizes, from 2.0 mm to 3.7 mm.

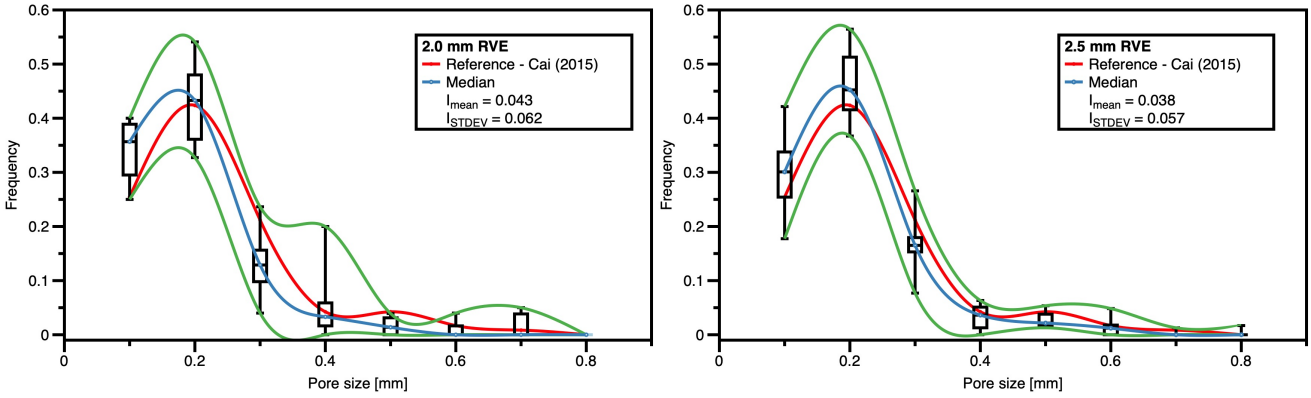

(a) (b)

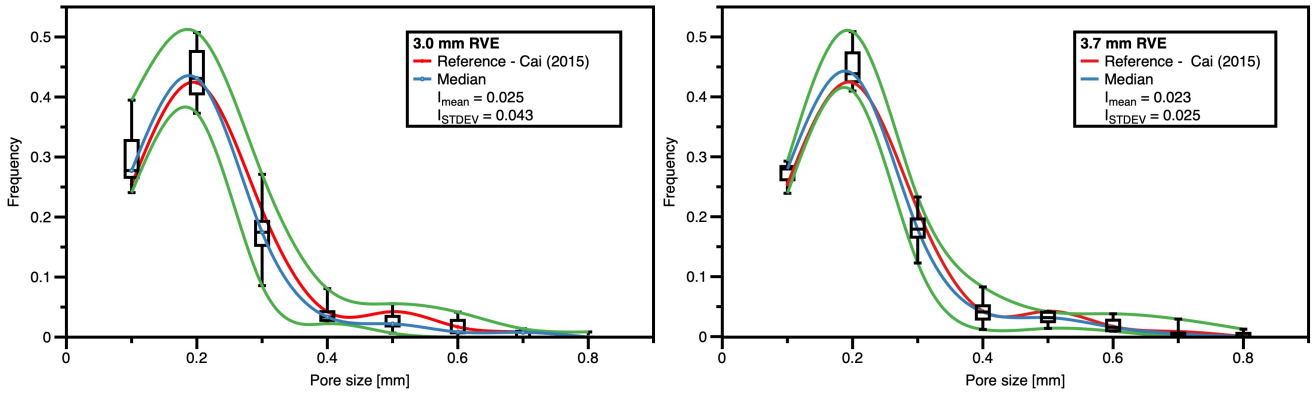

(c) (d)

Figure 9 – RVE Random porosity Distribution, 3.16% overall porosity. 9a - 9d 2.0 mm, 2.5 mm, 3.0 mm and 3.7 mm edge size, respectively.

At increasing edge size, distribution at each pore size is more accurate: a decreasing maximum and minimum values gap is delineated, while the median curve approximates the reference curve better. To check the quality of the statistical data, the weighted mean index I_{mean} and standard deviation index I_{STDEV} have been used:

$$I_{mean} = \frac{\sum_{i=1}^{N} |\bar{x}_i - w_i| \times w_i}{\sum_{i=1}^{N} w_i}; \qquad I_{STDEV} = \frac{\sum_{i=1}^{N} STDEV_i \times w_i}{\sum_{i=1}^{N} w_i} \tag{2}$$

where: $\bar{x}_i$ is the average value of each pore range size, w_i is the relative reference frequency as given in [21], and $STDEV_i$ is the standard deviation value of each pore range size. As the volume of the RVE increases, a convergence of the mean index is appreciated. An RVE with an edge size of $3.7mm$ is used for the numerical analyses.
Figure 10 compares true stress-strain curves of the Random Distribution RVE with the regular Matrix Distribution 3x3x3 RVE with an overall porosity of 3.16%.

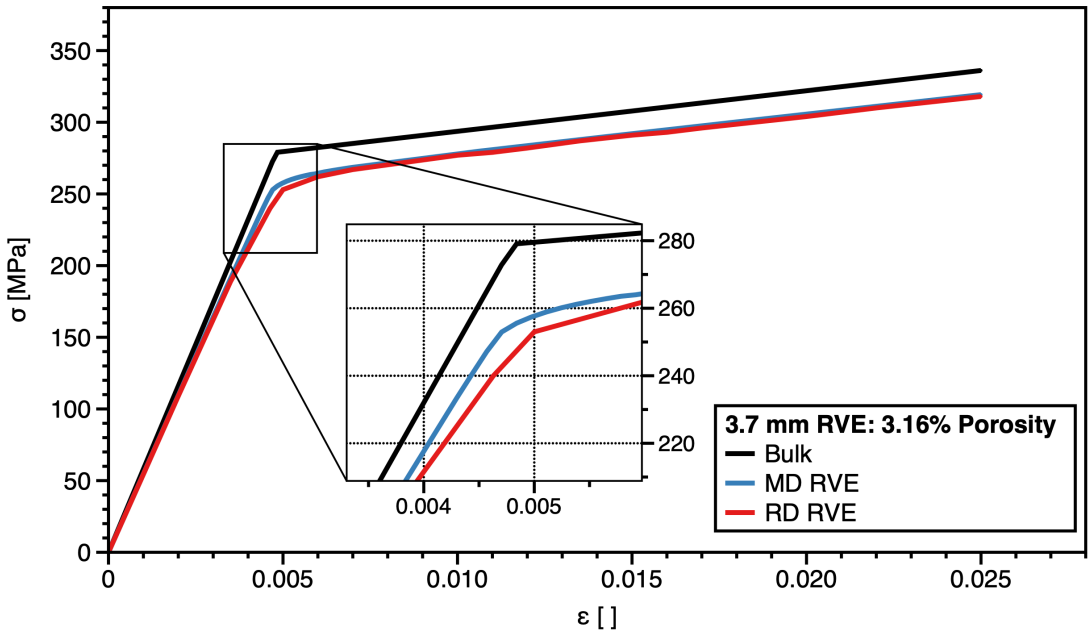

Figure 10 – RVE Matrix Distribution and Random pore Distribution stress-strain behaviour comparison.

The elastic modulus of the Random Distribution RVE is $54000MPa$ and the yield stress is $240MPa$. This marked reduction of the mechanical properties can be caused by the intersection of pores near which high stresses are recorded causing the material to reach the plastic hardening phase earlier. A map of normal stress distribution along the x-axis is reported in Figure 11. As expected, the highest stress values are recorded close to pore edges, thus confirming the importance of modelling random pore distribution to get accurate results.

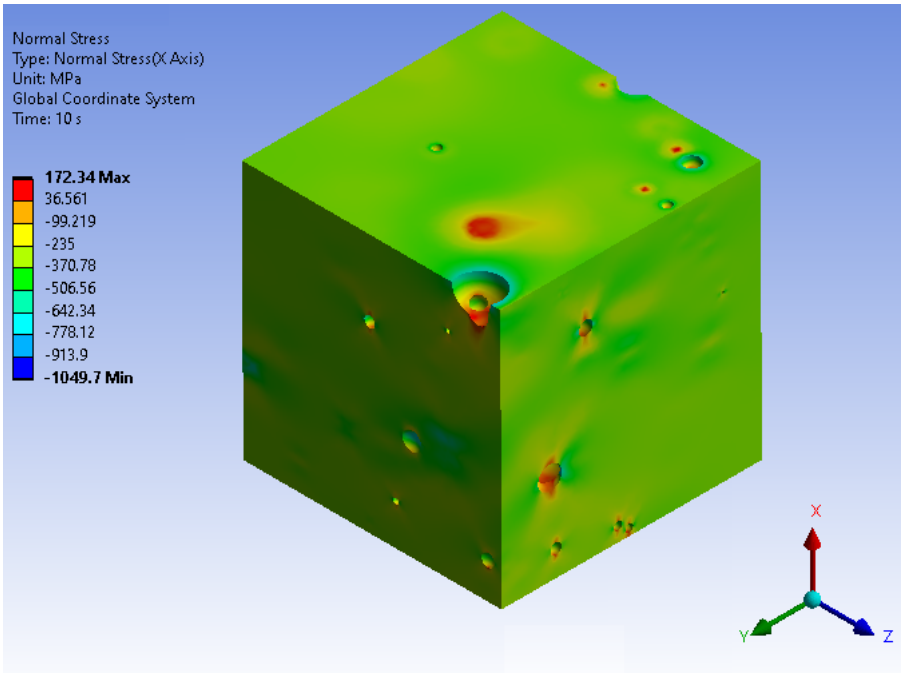

Figure 11 – Numerical results: Normal stress distribution, x-direction.

Finally, the accumulated Von Mises stresses frequencies at 0.5% strain of the Single Pore distribution, regular Matrix Distribution and Random pore Distribution are reported in Figure 12. Each curve is retrieved by counting the volume element percentage of the whole RVE exceeding a given value of stress.

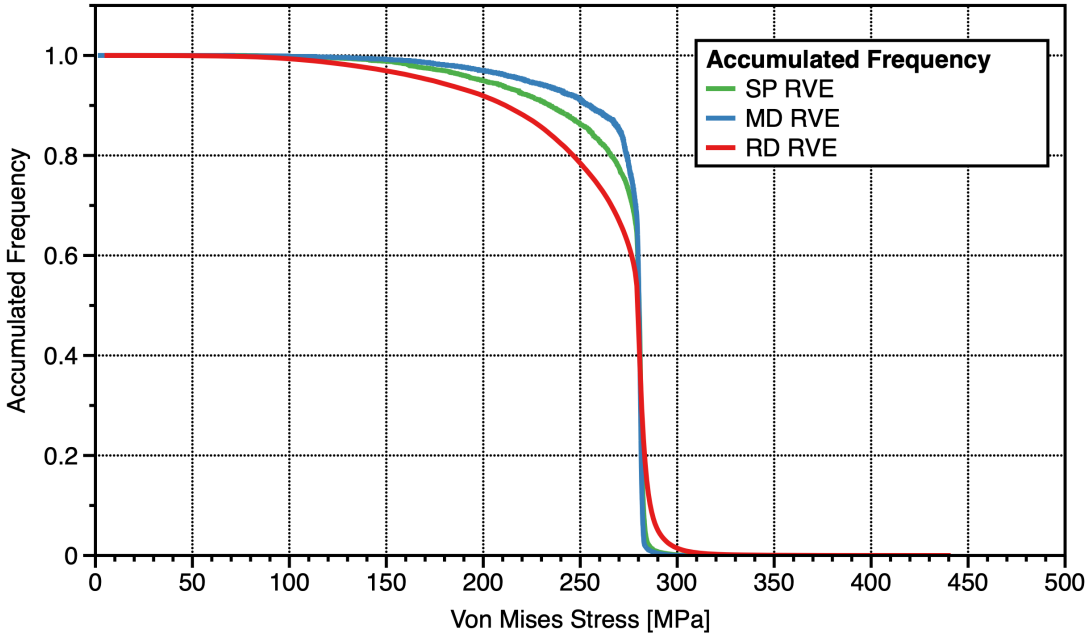

Figure 12 – Accumulated Von mises stress frequencies at 0.5% strain.

A higher probability is recorded for both the Single Pore RVE and the regular Matrix Distribution RVE than the Random pores Distribution RVE at the bulk yield stress of $279MPa$ or more. However, as expected, RD RVE presents peak stresses over $300MPa$ in a limited portion of volume fraction elements due to the presence of coalesced pores in the transverse direction of the load.

4. Conclusions

In this work, the Representative Volume Element like approach was used to numerically determine the stress-strain behaviour of an additively manufactured Selective Laser Melted AlSi10Mg impaired with pores.

To understand how pore distribution influences the overall behaviour of the component, the study analysed and compared multiple RVEs with different overall porosity values and in different spatial configurations. Through an in-house routine developed in Ansys APDL, multiple RVE models were generated in batch mode according to literature studies. Statistically, the procedure well approximates the reference distribution and can be easily modified for different materials and process parameters. The study confirms that overall porosity is one of the main parameters that drive the mechanical behaviour of the models: as the void volume fraction increases, the proportional limit decreases, with an almost linear trend, with lower yield strength values. Pore size and position also influence the mechanical response. A marked reduction of the elastic modulus and the yield strength is recorded for the RVE with a random porosity distribution configuration. Pores coalesced perpendicularly to the loading direction locally present high values of stresses anticipating the transition in the plastic region. The retrieved values are consistent with both theoretical results and literature studies on RVE used to predict the macroscopic response of porous metals.

The proposed Representative Volume Element like approach is easily extendable to different case studies and can be paired with in-situ monitoring and AI optimised process techniques allowing the designer to predict the constitutive relations of different materials and as a comparison tool with experimental tests once known their porosity distribution. This model can also be used as a first step for the homogenisation process in a multiscale analysis, considerably reducing the cost of numerical analyses and the necessity of multiple experimental tests. Proper double periodicity boundary conditions will be considered in future works to account for different loading scenarios. Furthermore, different constitutive relations will be studied to predict damage evolution and failure.

5. Copyright Statement

***Corresponding Author: Giuseppe Mantegna**
Faculty of “Engineering and Architecture” Kore University of Enna, Cittadella Universitaria - 94100 Enna, Italy
Phone Number: +393293953018
E-mail: giuseppe.mantegna@unikore.it

References

[1] Aboulkhair, N.T., Everitt, N.M., Ashcroft, I., and Tuck, C. Reducing porosity in alsi10mg parts processed by selective laser melting. *Additive manufacturing*, 1:77–86, 2014.

[2] Li, J.Z., Alkahari, M.R., Rosli, N.A.B., Hasan, R., Sudin, M.N., and Ramli, F.R. Review of wire arc additive manufacturing for 3d metal printing. *International Journal of Automation Technology*, 13 (3):346–353, 2019.

[3] Everton, S.K., Hirsch, M., Stravroulakis, P., Leach, R.K., and Clare, A.T. Review of in-situ process monitoring and in-situ metrology for metal additive manufacturing. *Materials & Design*, 95:431–445, 2016.

[4] McCann, R., Obeidi, M.A., Hughes, C., McCarthy, É., Egan, D.S., Vijayaraghavan, R.K., Joshi, A.M., Garzon, V.A., Dowling, D.P., McNally, P.J., et al. In-situ sensing, process monitoring and machine control in Laser Powder Bed Fusion: A review. *Additive Manufacturing*, 45:102058, 2021.

[5] Shamsaei, N., Yadollahi, A., Bian, L., and Thompson, S.M. An overview of Direct Laser Deposition for additive manufacturing; Part II: Mechanical behavior, process parameter optimization and control. *Additive Manufacturing*, 8:12–35, 2015.

[6] Wang, Y., Zheng, P., Peng, T., Yang, H., and Zou, J. Smart additive manufacturing: current artificial intelligence-enabled methods and future perspectives. *Science China Technological Sciences*, 63(9):1600–1611, 2020.

[7] Abd Aziz, N., Adnan, N.A.A., Abd Wahab, D., and Azman, A.H. Component design optimisation based on artificial intelligence in support of additive manufacturing repair and restoration: Current status and future outlook for remanufacturing. *Journal of Cleaner Production*, 296: 126401, 2021.

[8] Odegard, J. and Pedersen, K. Fatigue properties of an a356 (alsi7mg) aluminium alloy for automotive applications-fatigue life prediction. *International Journal of Fatigue*, 2(17):158, 1995.

[9] Shan, Z. and Gokhale, A.M. Representative volume element for non-uniform micro-structure. *Computational Materials Science*, 24(3):361–379, 2002.

[10] Chan, L.C., Lu, X., and Yu, K.M. Multiscale approach with rsm for stress–strain behaviour prediction of micro-void-considered metal alloy. *Materials & Design*, 83:129–137, 2015.

[11] Drugan, W.J. and Willis, J.R. A micromechanics-based nonlocal constitutive equation and estimates of representative volume element size for elastic composites. *Journal of the Mechanics and Physics of Solids*, 44(4):497–524, 1996.

[12] Hill, R. Elastic properties of reinforced solids: some theoretical principles. *Journal of the Mechanics and Physics of Solids*, 11(5):357–372, 1963.

[13] Hashin, Z. Analysis of Composite Materials—A Survey. *Journal of Applied Mechanics*, 50(3): 481–505, 09 1983. ISSN 0021-8936. doi: 10.1115/1.3167081.

[14] Gitman, I., Askes, H., and Sluys, L. Representative volume: Existence and size determination. *Engineering fracture mechanics*, 74(16):2518–2534, 2007.

[15] Gusev, A.A. Representative volume element size for elastic composites: a numerical study. *Journal of the Mechanics and Physics of Solids*, 45(9):1449–1459, 1997.

[16] Deng, Q., Bhatti, N., Yin, X., and Abdel Wahab, M. Numerical modeling of the effect of randomly distributed inclusions on fretting fatigue-induced stress in metals. *Metals*, 8(10):836, 2018.

[17] Takezawa, A., Kobashi, M., Koizumi, Y., and Kitamura, M. Porous metal produced by selective laser melting with effective isotropic thermal conductivity close to the hashin–shtrikman bound. *International Journal of Heat and Mass Transfer*, 105:564–572, 2017.

[18] Biswas, N. and Ding, J. Numerical study of the deformation and fracture behavior of porous ti6al4v alloy under static and dynamic loading. *International Journal of Impact Engineering*, 82: 89–102, 2015.

[19] Kanit, T., Forest, S., Galliet, I., Mounoury, V., and Jeulin, D. Determination of the size of the representative volume element for random composites: statistical and numerical approach. *International Journal of solids and structures*, 40(13-14):3647–3679, 2003.

[20] Liu, Y.J. and Chen, X. Evaluations of the effective material properties of carbon nanotube-based composites using a nanoscale representative volume element. *Mechanics of materials*, 35(1-2): 69–81, 2003.

[21] Cai, X., Malcolm, A.A., Wong, B.S., and Fan, Z. Measurement and characterization of porosity in aluminium selective laser melting parts using x-ray ct. *Virtual and Physical Prototyping*, 10(4): 195–206, 2015.

[22] Yu, W., Sing, S.L., Chua, C.K., and Tian, X. Influence of re-melting on surface roughness and porosity of alsi10mg parts fabricated by selective laser melting. *Journal of Alloys and Compounds*, 792:574–581, 2019.

[23] Majeed, A., Zhang, Y., Lv, J., Peng, T., Atta, Z., and Ahmed, A. Investigation of t4 and t6 heat treatment influences on relative density and porosity of alsi10mg alloy components manufactured by slm. *Computers & Industrial Engineering*, 139:106194, 2020.

[24] Yin, X., Chen, W., To, A., McVeigh, C., and Liu, W.K. Statistical volume element method for predicting microstructure–constitutive property relations. *Computer methods in applied mechanics and engineering*, 197(43-44):3516–3529, 2008.